Dielectronic recombination of N^{4+}

P. Glans,[1,*] E. Lindroth,[1] N. R. Badnell,[2] N. Eklöw,[2] W. Zong,[1] E. Justiniano,[3] and R. Schuch[1]

[1]*Atomic Physics, Physics Department, Stockholm University, Frescativ 24, S-104 05 Stockholm, Sweden*

[2]*Department of Physics and Applied Physics, University of Strathclyde, Glasgow G4 0NG, United Kingdom*

[3]*Department of Physics, East Carolina University, Greenville, North Carolina 27858*

(Received 30 April 2001; published 17 September 2001)

The dielectronic recombination spectrum of N^{4+} has been measured with high resolution and accuracy. The $1s^22p5l$ resonances in the energy range 0–1.6 eV were studied in detail. The experimental spectrum is compared with the results from four different calculations. An almost perfect agreement between the experiment and a calculation which combines relativistic many-body perturbation theory and complex rotation is found. The calculation provides accurate spectroscopic data for all fifty $1s^22p5l$ states. The literature value for the $1s^22p5s\ ^1P$ energy level is found to be off by more than 0.1 eV.

DOI: 10.1103/PhysRevA.64.043609 PACS number(s): 34.80.Lx, 31.15.Ar, 31.50.Df

I. INTRODUCTION

Dielectronic recombination (DR) is a fundamental process through which a free electron may be captured by an ion. It plays an important role for the dynamics of high-temperature laboratory and astrophysical plasmas. The process is resonant and, therefore, very sensitive to the atomic structure of the recombined ion. In recent years, heavy-ion storage rings equipped with electron coolers have made it possible to record DR spectra with high resolution and accuracy. The spectral quality obtainable today makes stringent tests of atomic structure calculations possible. In this paper, we present the DR spectrum for Li-like N^{4+}, which recombines into Be-like N^{3+}. The experimental spectrum is compared to theoretical spectra from four different computational models.

DR may be regarded as a two-step process. In the first step a doubly excited state is formed in the recombined ion through a resonant process involving the capture of a free electron and the simultaneous excitation of a bound electron, i.e., a reverse Auger process. In the second step the doubly excited state decays by emitting a photon to a state below the ionization threshold. The radiative stabilization is necessary to prevent the ion from autoionizing. In this work the following transitions are studied:

$$e^- + N^{4+}(1s^22s) \rightarrow N^{3+}(1s^22pnl) \rightarrow N^{3+}(1s^22snl) + \text{photon or } N^{3+}(1s^22pn'l') + \text{photon},$$

where $n \geqslant 5$ and $n' < 5$. In the first step, the innermost of the two active electrons remains within the same shell and it is therefore referred to as a $\Delta n = 0$ DR process. These transitions are in many cases the most important ones because they typically appear at fairly low center-of-mass (c.m.) energies and commonly give rise to the strongest resonances in the DR spectra.

Accurate measurements at low c.m. energies require well-aligned, cold electron and ion beams, which is achieved by using merged-beam techniques. The first reports of DR spectra from ''single-pass'' merged-beam experiments appeared in 1983 [1–3]. Since then the resolution and signal-to-noise ratio in this type of experiments have been vastly improved. One significant improvement was the implementation of ion storage rings equipped with so-called electron coolers. In such devices the ion beam can pass through the interaction region, that is the electron target, many times. The ion storage half-life varies from seconds to days, but is typically about tens of seconds. This time is sufficient to first use the electrons as a cooling agent for the circulating ion beam, and then to use them as a target for the recombination measurements. During the cooling phase, the ion-beam diameter shrinks from cm-size to about 1 mm and the longitudinal velocity and the velocity spread of the ions are tuned to those of the electrons in the center of the electron beam. The resolution in the recombination measurements is then primarily limited by the longitudinal and transversal temperatures of the electron beam.

During the past decade recombination spectra for a number of ions have been measured at storage-ring facilities. Many of these studies have been made on lithiumlike ions, such as C^{3+} [4], F^{6+} [5,6], Ne^{7+} [7], Si^{11+} [8], Cl^{14+} [9], Ar^{15+} [10], Ti^{19+} [11], Ni^{25+} [12], and Cu^{26+} [13]. Numerous investigations on Li-like ions were also made in single-pass experiments, recently, for example, on Au^{76+}, Pb^{79+}, Bi^{80+}, and U^{89+} [14]. Previous measurements of the $\Delta n = 0$ DR spectrum of Li-like N^{4+} have also been made in single-pass experiments [15,16]. Those investigations were made with modest resolution and signal-to-noise ratio. We present the first spectrum recorded at a storage ring for this system. The resolution and signal-to-noise ratio are considerably improved compared to the previous experiments. These improvements are essential for a critical test of theoretical results.

The interest in these Li-like ions stems from their rather simple electronic structure with two tightly bound $1s$ electrons and one loosely bound $2s$ electron. Because of this fairly simple electronic structure the Li-like ion beams are

*Permanent address: Department of Engineering, Physics and Mathematics, Mid-Sweden University, S-851 70 Sundsvall, Sweden.

free of any metastable ion fraction, the recombination spectra contain a limited number of resonances, and the formed doubly excited states in the corresponding Be-like ions comprise a pseudo-two-electron system with two active electrons outside a closed shell. Therefore, the calculations may be performed with pure *ab initio* methods. However, the electronic structure is still complicated enough to require a full many-body treatment and to match the experimental precision achieved today it is necessary to account for electron correlation to high orders as well as for relativistic and radiative effects.

In Sec. II some basic aspects of dielectronic recombination are discussed. The description of the experimental setup is made in Sec. III and of the computational models in Sec. V. In Sec. IV the data analysis is presented. The results are discussed in Sec. VI, and summarized in Sec. VII.

II. PROCESS

In DR a free electron is captured by an ion in a resonant process:

$$A^{q+}+e^{-}\rightarrow A^{(q-1)+**}\rightarrow A^{(q-1)+*}+\hbar\omega,$$

where A^{q+} denotes the initial state of the target ion, $A^{(q-1)+**}$ is the intermediate doubly excited state, and $A^{(q-1)+*}$ is any final state bound below the ionization threshold of the recombined ion.

The cross section for an isolated resonance at an energy position relatively far from threshold is given by a Lorentz profile

$$\sigma(\varepsilon_e)=\frac{1}{\pi}S\frac{\Gamma/2}{(E_d-E_{ion}-\varepsilon_e)^2+\Gamma^2/4}, \tag{1}$$

where ε_e is the relative energy of the electron, E_{ion} is the binding energy of the initial state in the target ion, E_d is the energy and Γ the natural lifetime width of the doubly excited state, and S is the strength of the resonance. That the resonance is isolated implies that there are no interference effects with overlapping resonances of the same symmetry or with transitions occurring directly from the initial state to the final states, i.e., radiative recombination channels. The resonance may be considered to be far from threshold if $\Gamma\ll(E_d-E_{ion})$. In this work, all the resonances can be considered to be isolated and far from threshold.

The integrated cross section, or strength, S is given by

$$S=\int\sigma(\varepsilon_e)d\varepsilon_e=\frac{\hbar^3\pi^2}{2m_e(E_d-E_{ion})}\frac{g_d}{g_i}\frac{A^a_{i\rightarrow d}\Sigma_s A^{rad}_{d\rightarrow s}}{A^a+\Sigma_s A^{rad}_{d\rightarrow s}}, \tag{2}$$

where m_e is the electron mass, g_i is the multiplicity of the initial target state, and g_d the multiplicity of the doubly excited intermediate state. $A^a_{i\rightarrow d}$ is the transition rate into the doubly excited state d, and $A^{rad}_{d\rightarrow s}$ is the radiative transition rate from state d (independent of the magnetic substate m_d), obtained after summation over magnetic substates of state s. The sum over states s includes all states below the ionization threshold. A^a is the total Auger transition rate from level d. The doubly excited states studied in this work are all situated below the second ionization threshold and, therefore, Auger decay can only occur to the ground state of the target ion. This means that $A^a=A^a_{i\rightarrow d}$. Furthermore, for almost all the doubly excited states the Auger rate A^a is much larger than the radiative rate $A^{rad}_{d\rightarrow s}$ and as a consequence the strength of the resonance depends mainly on the radiative rate, whereas the natural width of the resonance depends mainly on the Auger rate.

In the measurements a rate coefficient is measured as a function of relative energy E_{rel}. The rate coefficient α_R is the measured rate R normalized by the ion and electron currents:

$$\alpha_R=\frac{R}{N_i n_e L_i/L_r}\gamma^2. \tag{3}$$

In this expression N_i is the ion current, n_e the electron density in the interaction region, L_i the length of the interaction region, L_r the circumference of the storage ring, and γ the relativistic Lorentz factor ($\gamma\approx 1$).

The measured rate coefficient is related to the total cross section σ_{tot} by

$$\alpha_R(v_{rel})=\int\sigma_{tot}(v)v f(\vec{v},v_{rel})d\vec{v}, \tag{4}$$

where $f(\vec{v},v_{rel})$ is the distribution of the electron velocity $\vec{v}$, with magnitude v, relative to the ions around the average longitudinal center-of-mass velocity v_{rel}. Since the electron mass is much smaller than the ion mass, $v_{rel}=(2E_{rel}/m_e)^{1/2}$ in the nonrelativistic limit, and the velocity distribution is set by the distribution of the electrons. In merged-beam experiments this can be described by a ''flattened'' Maxwellian distribution [17] with different temperatures in the longitudinal $T_\parallel$ and transversal $T_\perp$ directions,

$$f(\vec{v},v_{rel})=\frac{m_e}{2\pi kT_\perp}\exp\left[-\frac{m_e v_\perp^2}{2kT_\perp}\right]\times\left(\frac{m_e}{2\pi kT_\parallel}\right)^{1/2}\times\exp\left[-\frac{m_e(v_\parallel-v_{rel})^2}{2kT_\parallel}\right], \tag{5}$$

where k is the Boltzmann constant, and $v_\parallel$ and $v_\perp$ are the longitudinal and transversal components of $\vec{v}$. The term flattened refers to the fact that $T_\parallel\ll T_\perp$.

In merged-beam experiments the electron density in the interaction region is low enough that recombination processes involving more than one free electron, such as three-body recombination, can be neglected. This means that the only other recombination process, besides DR, that give a significant contribution is radiative recombination (RR). In RR the free electron is captured in a nonresonant one-step (reverse photoionization) process, where the excess energy is carried away by an emitted photon:

$$A^{q+}+e^{-}\rightarrow A^{(q-1)+*}+\hbar\omega.$$

The cross section for RR into a Rydberg level n can be fairly accurately determined using the semiclassical formula derived by Kramers [18],

$$\sigma_n(\varepsilon_e)=\frac{32\pi}{3\sqrt{3}}\alpha^3 a_0^2\frac{q^4R_\infty^2}{n\varepsilon_e(q^2R_\infty+n^2\varepsilon_e)}, \tag{6}$$

where α is the fine-structure constant, a_0 the Bohr radius, q the initial ion charge state, and R_∞ the Rydberg energy. The semiclassical formula works fairly well even for ions with electrons already bound, provided the occupied shells are not counted in the sum over the final states. Furthermore, in the experiments the recombined ions are charge separated from the primary ion beam by a strong dipole magnet, and the motional electric field experienced by the ions is enough to field ionize loosely bound electrons. The sum over the final states, therefore, becomes limited to a maximum value n_{max} [19],

$$n_{max}=\left(\frac{6.2\times10^{10}q^3}{F}\right)^{1/4}, \tag{7}$$

where F is the motional electric field (in V/m).

It should be noted that the final states reached in RR can also be reached via DR and, therefore, quantum-mechanical interference between the RR and DR pathways is, in principle, possible. However, observable interference effects between RR and DR are very unlikely, especially since the photon energy is not detected in the merged-beam experiments, and hence many final states contribute to the cross section $\sigma(\varepsilon_e)$. In fact, interference effects have not been observed in any merged-beam experiment so far. Therefore, for almost all systems, one can treat RR and DR as two separate, independent processes and the rate coefficients can be calculated separately.

III. EXPERIMENT

The experiments were made at the Manne Siegbahn laboratory in Stockholm using the ion storage ring CRYRING. The N^{4+} ions were produced in an electron-beam ion source and extracted at 40 keV/amu. The ion beam was transported from the source to the ring via a radio-frequency quadrupole, which was used to preaccelerate the ions to 300 keV/amu. The final acceleration to 8 MeV/amu of the ions took place in the ring.

The ring is equipped, on one of its straight sections, with an electron cooler. The electron cooler provides a magnetically confined electron beam which overlaps with the ion beam over an effective length of about 0.8 m. The electron beam is adiabatically expanded from a beam diameter of 4 mm at the cathode to 4 cm in the interaction region by a reduction of the magnetic field with a factor of 100 from 3 T at the cathode to 0.03 T in the interaction region. The adiabatic expansion is used in order to reduce the transversal temperature $kT_\perp$ of the electron beam. At the cathode the temperature can be assumed to be Maxwellian with $kT=0.1$ eV. In the longitudinal direction the electron beam is kinematically compressed, due to the acceleration of the electrons, and the temperature $kT_\parallel$ in this direction is reduced to about 0.1 meV. The transversal temperature, on the other hand, is lowered only because of the adiabatic expansion. The CRYRING cooler, which uses a superconducting magnet, provides an exceptionally large expansion factor of 100 and thereby a low transversal temperature of the electron beam. The optimal value of $kT_\perp$ is the original temperature divided by the expansion factor, i.e., 1 meV. However, the results from a DR measurement on F^{6+} indicates a somewhat higher value of $kT_\perp=3.0$ meV [20].

In the DR measurements the electron cooler fills two purposes. First, the cooler is used to cool the ions after they have been accelerated. The electron beam is then set to have the same average velocity as the ions, and the cold electrons thereby, through repeated collisions with the ions, significantly reduce the longitudinal and transversal velocity spread and the diameter of the ion beam. The second purpose of the cooler is to provide an electron-beam target for the ions that enables recombination processes. To fill this purpose the energy of the electrons is varied in a systematic way after that the injection and cooling phases are completed. In our measurements the energy of the electrons is varied slowly in a zigzag pattern. After each zigzag scan, which was set to take 4 sec, the ion beam was dumped and a new injection was made. For each recorded spectrum the same measuring cycle was repeated many times.

The ions that recombined with an electron in the cooler are charge separated from the primary ion beam by the first dipole magnet after the cooler and are detected as events by a 100% efficiency surface barrier detector positioned just behind the dipole magnet. For each detected event three values are recorded in a list-mode file. These values correspond to the pulse height from the surface barrier detector, the cathode voltage on the electron gun, and the time at which the event occurred in the measuring cycle. The latter value is a digital value generated by a function generator, which is synchronized to the measuring cycle.

The electron current was kept at 87 mA during the measurements. The ion-beam current was measured using a current transformer. Typically the ion current was about 1 μA, after acceleration and the half-lifetime was measured to be 16 sec.

IV. DATA ANALYSIS

To obtain a spectrum, showing the rate coefficient α_R as a function of relative energy E_{rel}, from the list-mode data requires several steps of data analysis. In this section the data analysis procedure will be briefly outlined. A more detailed account of the procedure can be found in Ref. [7].

A list-mode data file contains events from many measuring cycles. Injection, cooling, and the subsequent measurement scan appear at identical times in each of the cycles and, hence, at a certain ''cycle time'' the relative energy E_{rel} is always the same. Therefore, the data analysis aims at generating the final spectrum by obtaining for each time channel (which correspond to a specific cycle time) α_R and E_{rel}.

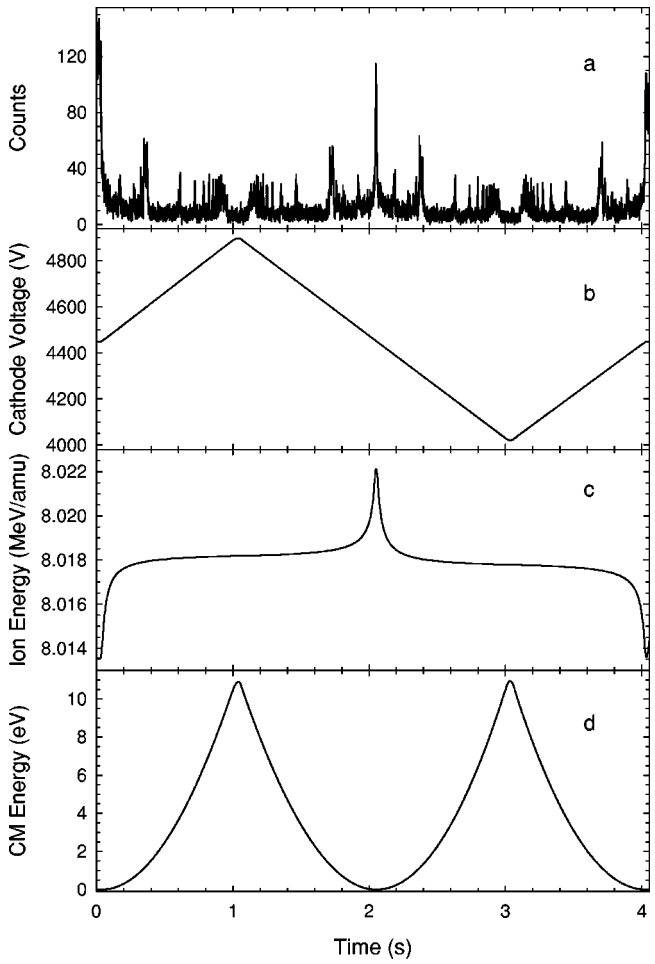

FIG. 1. (a) A time spectrum obtained by the zigzag energy scan of the electrons shown in (b). (c) The corresponding variation of the ion energy as a function of time. (d) The relative energy as a function of time. Note that the raw-data spectrum contains four parts that cover the same energy range and that the RR peak, in the middle of the raw-data spectrum, precisely defines the time at which the electron velocity equals the ion velocity.

A. Relative energies

There were three sets of list-mode data recorded during the beam time. One set of data covered relative energies up to about 11 eV, and two covered a narrower range up to about 1.6 eV. The former data set, hereafter referred to as the wide data set, covers all the $2pnl$ resonances, whereas the latter, narrow data sets only cover the $2p5l$ resonances.

A ''time spectrum'' is generated from the list-mode data by finding the total number of recombined ions as a function of (cycle) time. In Fig. 1(a) the time spectrum from the wide data set is shown. Below, in Fig. 1(b), it is shown how the cathode voltage varies with time. The cathode voltage function is also derived from the list-mode data. During the first half of the zigzag scan the electrons are faster than the ions, whereas in the second half they are slower than the ions. The point at which the average electron and ion velocities are the same can easily be determined by the fact that RR is most likely when the velocities are the same. In the time spectrum [Fig. 1(a)], a distinct RR peak is observed at about 2.05 sec.

The real electron energy E_e is related to the cathode voltage U_{cath} by

$$E_e = e(U_{cath} + U_{sp}), \tag{8}$$

where e is the elementary charge and U_{sp} is the space-charge potential, which is modeled by the formula

$$U_{sp} = -(1-\zeta)\frac{I_e r_c m_e c^2}{v_e e}\left[1 + 2\ln\left(\frac{b}{a}\right) - \left(\frac{r}{a}\right)^2\right], \tag{9}$$

where I_e is the electron current, r_c is the classical electron radius, c is the speed of light, v_e is the electron velocity, r is the distance from the center of the electron beam axis, and a and b are the radii of the electron beam and the cooler tube, respectively. The parameter ζ accounts for the fact that residual ions trapped in the electron beam reduce the magnitude of the space-charge potential. The number of trapped ions changes with the vacuum pressure, electron energy, and electron density. However, in the present work, where the variations in electron energy and density are fairly small, ζ is assumed to be a constant. In addition, $r=0$ is assumed, since the ion beam after cooling is narrow and centered in the middle of the electron beam.

When the average velocities of the electrons and ions are different, the electron beam will exert a drag force on the ions. The force will be largest when the velocity detuning is small. The drag force is large enough to cause the ion energy E_i to vary during the slow zigzag scan used, and it becomes necessary to estimate how the ion energy varies with time. This is done by using a differential equation based on Newton's second law with a free parameter η. This parameter is chosen so that the ion and electron velocities match at the time where the RR peak occurs. In Fig. 1(c) the variation of the ion energy with time is shown. The figure shows that the ions are accelerated when the electrons are faster, they reach their maximum energy when the velocities match, and they are decelerated when the electrons become slower than the ions.

The center-of-mass energies E_{rel} are obtained from the laboratory energies E_e and E_i by the relativistic formula

$$E_{rel} = [(E_i + E_e + m_i c^2 + m_e c^2)^2 - (\sqrt{E_i^2 + 2m_i c^2 E_i} + \sqrt{E_e^2 + 2m_e c^2 E_e})^2]^{1/2} - m_i c^2 - m_e c^2, \tag{10}$$

where m_i is the ion mass. In Fig. 1(d) the relative energy E_{rel} is plotted as a function of time. Note that the zigzag scan leads to four spectral parts that cover the same energy range. The four spectra generated should be identical in the center-of-mass frame, and hence the resonance positions should ideally be the same in all four spectra. This matching criterion is used to further optimize free parameters in the previous steps of the data analysis. In the present study the previous steps were not sufficient to make the four spectra overlap perfectly. The main reason for this is probably small uncertainties in the cathode voltage function. However, by linearly stretching or compressing the energy values for three of the parts to

maximize the overlap with the fourth part, an almost perfect overlap over the entire energy range was achieved.

B. Rate coefficients

The rate coefficient in each time channel is calculated from Eq. (3). In this equation, the rate R is the number of counts divided by the total acquisition time for the time channel, where the acquisition time equals the time length of one channel times the number of measuring cycles. The electron density is obtained from the electron current, assuming a homogeneous electron distribution in the beam. The largest uncertainty in the determination of the rate coefficients stems from the uncertainty in the ion current value. To minimize this error the ion current was carefully measured simultaneously with one of the narrow data sets. The exponentially decaying beam intensity during the 4-sec scan was taken into account. It can be estimated to be in total 20%. The decay can be seen from the RR intensities at beginning, center, and end of a time spectrum in Fig. 1(a). The systematic error introduced by the uncertainties in the ion current is estimated to be less than 10%. The uncertainty in the interaction length L_i might also give a significant systematic error, which is of the same order. In other words, the experimentally determined rate coefficients might have a systematic error of up to 20%.

C. Improvement of energy scale

When α_R and E_{rel} have been determined for each time channel a final spectrum can be generated for the data set. The number of channels is reduced by averaging over data points which have approximately the same E_{rel} values. In addition, a constant background is subtracted. This background stems from detected ions which have captured an electron in collisions with rest gas atoms or molecules in the electron cooler section.

The error in the energy scale is typically less than a few percent. The fact that linear corrections were sufficient to achieve a very good overlap between the four spectral parts (this was true for all three data sets) indicates that the error in the energy scale can be substantially reduced by a linear correction.

One possibility would be to use the $(2pnl_j)$ series limits for energy calibration. In the DR spectrum the positions of the series limits are accurately known from optical data [21]. They correspond to the $2s$-$2p_{1/2}$ and $2s$-$2p_{3/2}$ splittings in N^{4+}, which are 9.97617 and 10.00824 eV, respectively. However, accurate calibration using the series limits is difficult since the limits are not sharp features in the spectra. Therefore, the experimental energy scale is calibrated using the positions of DR resonances close to the series limits. The spectrum from the AUTOSTRUCTURE (AS) [22] calculation is used. Figure 2 shows how the DR spectrum, from the wide data set, compares with the theoretical AS spectrum, in the energy region where DR resonances into high Rydberg states ($n \geqslant 6$) contribute, after the experimental energy scale was linearly stretched. Here it is important to remark that the observed energy splittings were used in the AS calculations, and so the Rydberg series converge to the observed limits.

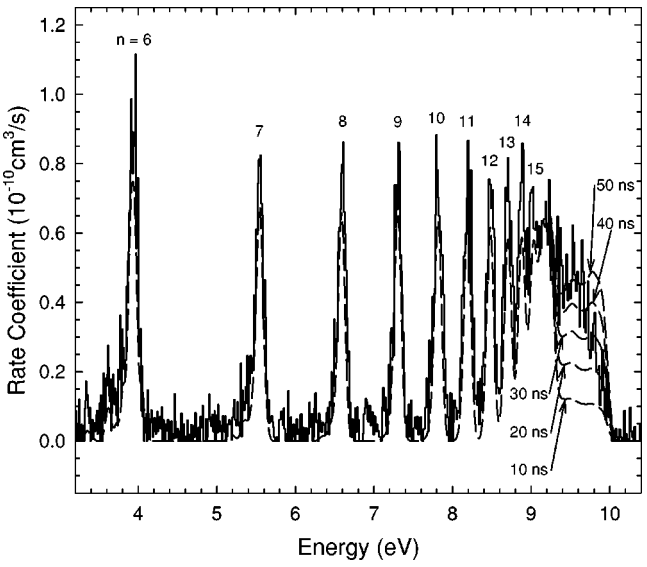

FIG. 2. The DR spectrum in the energy region covering the $2pnl$ resonances from $n=6$ to the series limits ($n=\infty$). The dashed lines are obtained from the AS calculation using flight times of 10, 20, 30, 40, and 50 ns. The solid line is the experimental spectrum. The experimental energy scale has been linearly adjusted so that the resonance positions fit the theoretical ones near the series limits. See the text for more details.

Thus the calculated and observed high-n resonances should be in close agreement. It is only as we drop to low-lying resonances which interact strongly with the core that we might expect to, and indeed do, observe deviations. The energy scales in the DR spectra from the narrow data sets are then calibrated (also using a linear correction) against the calibrated spectrum from the wide data set.

After calibration we estimate the uncertainty of the experimental energies to be less than 1% and not more than 5 meV in the region where the $2p5l$ resonances occur.

V. COMPUTATIONAL MODELS

We have used and compared four different computational approaches to calculate the low relative energy recombination spectra. The different approaches are discussed below. The resonances situated up to $\sim$1.6 eV above the ionization threshold of N^{3+}, seen in Fig. 3 and again in Figs. 4 and 5, are due to doubly excited states above N^{4+} $(1s^2 2s)$, but bound below N^{4+} $(1s^2 2p_j)$ and dominated by $2p_j 5l'_j$ configurations. The resonances are expected at relative electron energies $\varepsilon_e = E(1s^2 2p) + \Delta E - E(1s^2 2s_{1/2})$. ΔE can be regarded as the binding energy of the ''outer'' electron. The fine-structure splitting of the $2p$ state is $\sim$0.03 eV, considerably larger than the experimental resolution. Since N is a rather light element, where the electron-electron interaction still dominates over the spin-orbit interaction, the resonances will not be of either $2p_{1/2}$ or $2p_{3/2}$ character, but a mixture of the two. Accurate values for the $(2p_j - 2s)$ splittings are important ingredients to obtain accurate positions for the resonances. The results obtained when the binding energies of the $N^{4+}(1s^2 2l_j)$ states are calculated with relativistic

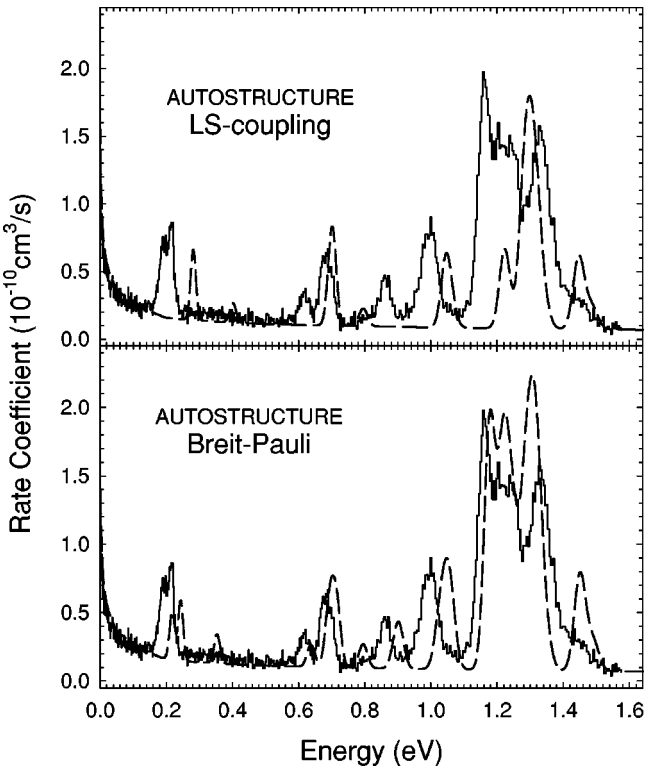

FIG. 3. The full line histogram shows the experimental spectrum in the low-energy region, where the $2p5l$ DR resonances contribute. The dashed curves show theoretical spectra obtained using the AUTOSTRUCTURE method, discussed in Sec. V A. In the upper graph the calculations were performed within the LS coupling and in the lower the Breit-Pauli approximation was used.

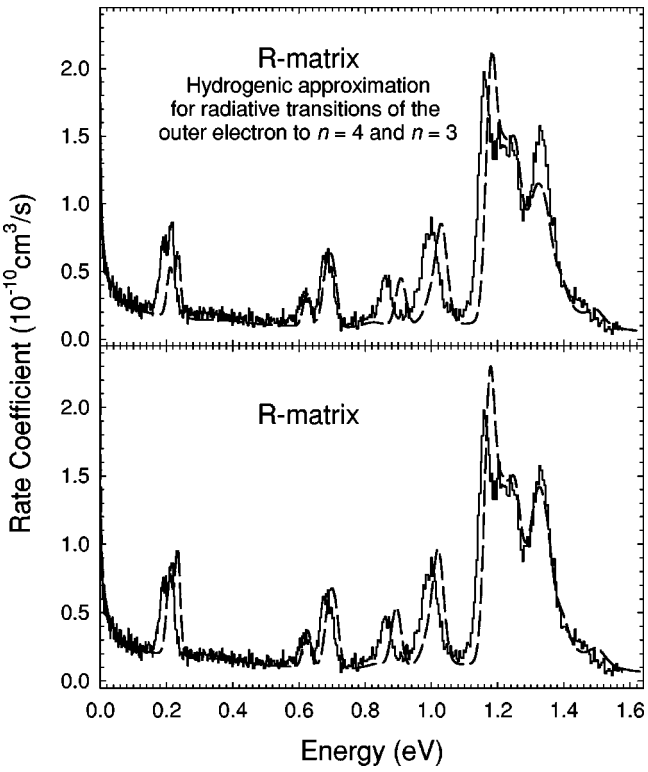

FIG. 4. Same as in Fig. 3 but for calculations using the R-matrix method, discussed in Sec. V B.

many-body perturbation theory in the all-order formulation within the single- and double-excitation scheme described in Refs. [23,24] are shown in Table I.

A. AUTOSTRUCTURE

The two graphs on Fig. 3 show the comparison between experiment and AS calculations [22]. In the upper graph, the calculation is performed within LS coupling. In the lower graph, the Breit-Pauli approximation is used, allowing for spin-orbit induced mixing of different LS symmetries. As a result several new peaks appear. This result underlines the importance of allowing for recombination also through relativistically forbidden channels even in very light elements. The reason is the huge difference between autoionization rates and radiative rates (see Table II). Indeed, the former dominates over the latter even for the states which are most stable against autoionization. Since the recombination strength is proportional to the weakest of these decay channels, as shown by Eq. (2) the autoionization can vary by several orders of magnitude without any noticeable effect on the recombination strengths. In both calculations shown in Fig. 3, the observed $2p_j$-$2s$ splittings are used as input. In the case of AS performed within the LS coupling (upper panel in Fig. 3), the two $2p_j$-levels are LS averaged. Equation (2) was used to obtain the strength contributed from each resonance.

B. R matrix

The results in Fig. 4 are from a Breit-Pauli R-matrix close-coupling calculation [25], and show the effect of describing the continuum–Rydberg electron nonperturbatively as well as allowing for interacting resonances and interference between DR and RR, although these latter effects can be expected to be very small [26]. In the upper part of the figure, the $5\rightarrow4$ and $5\rightarrow3$ radiative transitions are calculated within a hydrogenic approximation. In the lower panel

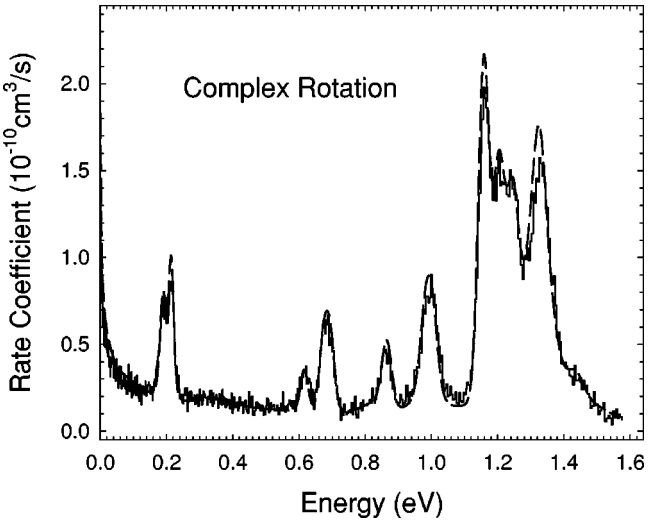

FIG. 5. Same as in Fig. 3, but for calculations using the complex rotation method, discussed in Sec. V C.

TABLE I. The contributions to the $2p_{1/2}$-$2s_{1/2}$ and $2p_{3/2}$-$2s_{1/2}$ splittings in N^{4+}.

	$2p_{1/2}$-$2s_{1/2}$ (eV) [a]	$2p_{3/2}$-$2s_{1/2}$ (eV) [a]
Dirac-Fock	10.0806	10.1176
Δ Dirac-Fock-Breit	0.0037	−0.0022
Coulomb correlation	−0.1028	−0.1021
Breit correlation	0.0004	0.0005
Mass polarization	−0.0015	−0.0015
Radiative corrections, H like [b]	−0.0056	−0.0054
Screening of radiative corrections [c]	0.0020	0.0019
Total	9.9766	10.0088
Experiment [d]	9.97617	10.00824

[a]1 a.u.$=27.211\,396\,M/(M+m_e)$ eV.
[b]Johnson and Soff [35].
[c]The $2s_{1/2}$ and $2p_{1/2}$ results are from McKenzie and Drake [36]. The $2p_{3/2}$ result is estimated from Blundell [37] by Z^3 scaling.
[d]Reference [21].

all radiative transitions are calculated in the *R* matrix method. In either case, the shape and magnitude of the peaks are now in much better agreement with experiment than in the case of the AS calculations of Fig. 3. The full *R*-matrix calculation shows a clearly better agreement with the experimental results. There is still, however, a shift in energy-position for several of the peaks which might be attributed to correlation in the doubly excited states. Also here the observed $2p_j$-$2s$ splittings are used as input.

C. Many-body perturbation theory calculation

The result obtained with relativistic many-body perturbation theory in an all-order formulation combined with complex rotation is shown in Fig. 5. Its agreement with the experimental results is remarkable. Equation (2) was used to obtain the strength contributed from each resonance. The method was used earlier on several other lithiumlike systems such as argon, neon, and carbon [10,27,4].

The $2p_j$-$2s$ splittings were calculated, and are presented in Table I. The calculation of resonance positions require the interaction between each of the outer electrons and the $1s^2$ core as well as the interaction between the valence electrons.

The autoionizing character of the doubly excited states appear when the valence-valence interaction is turned on. It pushes the states up above the threshold and is also responsible for the decay to the $2s\varepsilon l_j$ continua. To be able to describe autoionizing states, a description of the continuum of the outgoing electrons is needed. These functions are not square integrable, and *complex rotation* is used to represent the states in a limited cavity. The combination of many-body perturbation theory and complex rotation was used earlier in the nonrelativistic case [28,29], as well as in the relativistic case [10,27,4]. The method of complex rotation, where the radial coordinates in the Hamiltonian are rotated, $r \rightarrow re^{i\theta}$, has been used for a long time by many groups to account for the instability of autoionizing states; see, e.g., Refs. [30–32]. The method directly gives the autoionization width of the doubly excited state as the imaginary part of a complex binding energy. The real part of the energy corresponds to the position of the state. As in the *R*-matrix approach the effect of the continuum is accounted for nonperturbatively here.

The 18 $2p_j5l'_{j'}$ configurations which dominate the first resonances above the ionization threshold in N^{3+} are close in energy, and mix strongly. A general formulation of many-body perturbation theory which can handle degenerate or quasidegenerate, so called, *model spaces*, was developed by Lindgren [33], and was also discussed in connection to doubly excited states [34]. The idea behind the concept of an *extended model space* is that certain strongly coupling configurations, forming the *model space*, are included through a direct diagonalization of the Hamiltonian, while other configurations are included by perturbation theory. The perturbation expansion can be carried on to all orders, and can further be assumed to converge quickly if the model space is well chosen. This method is capable of treating the correlation between the two outer electrons more or less exactly, and has been used here. The agreement with experiment is very good. Some resonances were also measured with optical methods [21], and in most cases these values also agree very well with the calculation. This is, e.g., the case for the three $^3P^o$ states, giving rise to the first resonance around 0.2 eV for which the *R*-matrix method shows a slight offset.

The calculation is completely relativistic and thus within the *jj*-coupling scheme. To obtain a better understanding of the character of the resonances we have projected them onto a *LS* coupled basis, and the results are displayed in Table II. As can be seen, most resonances are well described by *LS* coupling. Still, resonances which would not exist nonrelativistically show up quite noticeably. For example, the $2p5p$ resonance at $\sim$0.62 eV is to 96%, of $^1P_1^e$ symmetry. This symmetry cannot autoionize. The small spin-orbit induced admixture of *S* and *D* symmetries causes the state to be weakly autoionizing, but the rate is 1 to 2 orders of magnitude slower than that from resonances dominated by these symmetries ($2p5p\ ^3S_1$, or $^3D_1$). The radiative rate is, however, still much slower. Since the recombination strength is

TABLE II. Calculated resonance positions, widths and strength for the $N^{3+}(2p5l)$ resonances, from the many-body perturbation theory calculation discussed in Sec. V C. The second column gives the dominating *LS* term and the extent to which it describes the state. The autoionization rate is denoted with A^a and the radiative rate with A^{rad}.

Config.	Term	to%	J	Resonance position Calculated (eV)	Optical [21,38] (eV)	Width (eV)	A^a ($nsec^{-1}$)	A^{rad} ($nsec^{-1}$)	Strength (10^{-20} eV cm^2)
$2p5s$	^3P	100	0	0.1849	0.1846	0.004	6161	2.26	1.51
		99.5	1	0.1942	0.1958	0.005	7821	2.25	4.30
		100	2	0.2164	0.2165	0.004	5985	2.26	6.45
$2p5s$	^1P	99.5	1	0.3496	0.4564	0.142	215976	3.37	3.58
$2p5p$	^1P	96.2	1	0.6186	0.6174	0.0002	283	2.47	1.47
$2p5p$	^3D	96.3	1	0.6720	0.6699	0.0013	1942	1.93	1.06
		99.6	2	0.6804	0.6779	0.0013	1975	1.97	1.79
		100	3	0.6980	0.6952	0.0013	1952	1.98	2.45
$2p5p$	^3S	98.8	1	0.8238		0.065	99091	2.47	1.11
$2p5p$	^3P	99.9	0	0.8553	0.8573	0.0002	316	2.38	0.34
		98.8	1	0.8638	0.8607	0.003	5249	2.36	1.01
		99.4	2	0.8721	0.8682	0.000007	10	2.37	1.36
$2p5d$	^3F	93.7	2	0.9740		0.028	42889	1.61	1.02
$2p5p$	^1D	99.4	2	0.9853		0.002	2818	3.06	1.92
$2p5d$	^3F	99.5	3	0.9869		0.031	46951	1.67	1.47
		99.9	4	1.0021		0.031	46976	1.67	1.86
$2p5d$	^1D	93.6	2	1.0069		0.003	4073	3.38	2.08
$2p5d$	^3D	98.2	1	1.1542	1.1522	0.0007	1074	7.84	2.50
		96.0	2	1.1578	1.1552	0.0015	2318	7.69	4.09
		99.6	3	1.1653	1.1652	0.0003	439	7.94	5.80
$2p5f$	^1F	84.7	3	1.1997		0.0007	1071	2.29	1.65
$2p5f$	^3F	98.8	2	1.2039		0.000010	15	2.31	1.02
		84.2	3	1.2071		0.003	4943	2.12	1.52
		98.2	4	1.2096		0.003	5228	2.30	2.12
$2p5f$	^3P	96.1	2	1.2139	1.2155	0.033	49428	4.92	2.51
		98.3	1	1.2223		0.033	50691	5.02	1.52
		100	0	1.2265		0.034	51611	5.09	0.51
$2p5g$	^3G	94.9	3	1.2462		0.000007	11	1.44	0.88
		51.8	4	1.2462		0.000003	4	1.44	0.93
$2p5g$	^1G	50.7	4	1.2505		0.003	4032	1.44	1.28
$2p5g$	^3G	92.8	5	1.2507		0.003	4005	1.44	1.56
$2p5f$	^3G	98.1	3	1.2556		0.070	106191	2.34	1.61
		87.6	4	1.2615		0.071	107817	2.20	1.94
		100	5	1.2773		0.074	112141	2.36	2.52
$2p5f$	^1G	88.4	4	1.2952		0.076	115558	1.63	1.40
$2p5g$	^3H	92.8	4	1.2992		0.029	43334	1.44	1.23
		52.0	5	1.2995		0.029	43388	1.44	1.51
$2p5p$	^1S	99.9	0	1.3158		0.171	260509	2.02	0.19
$2p5g$	^3F	94.8	4	1.3180		0.00006	92	1.44	1.20
$2p5g$	^1F	53.2	3	1.3181		0.00004	66	1.46	0.94
$2p5g$	^3H	100	6	1.3187		0.031	47245	1.44	1.75
$2p5g$	^1H	55.9	5	1.3190		0.031	47284	1.44	1.48
$2p5g$	^3F	99.9	2	1.3330		0.00007	109	1.44	0.66
		56.2	3	1.3332		0.00004	59	1.44	0.91
$2p5f$	^3D	98.5	3	1.3343		0.0011	1697	2.33	1.51
		90.9	2	1.3413		0.0011	1634	2.23	1.03
		100	1	1.3500		0.0011	1727	2.35	0.65
$2p5d$	^1F	99.5	3	1.3632		0.117	177221	9.88	6.28
$2p5f$	^1D	91.0	2	1.3697		0.0006	944	2.07	0.93
$2p5d$	^1P	99.7	1	1.4409	1.4384	0.032	49273	5.96	1.54

proportional to the weakest of these decay channels [see Eq. (2)], it is more or less unaffected by the fact that recombination through this channel is non-relativistically forbidden.

VI. DISCUSSION

Figure 2 shows that the calculated rate coefficients for the $n \geqslant 6$ resonances appear to be about 25% lower than the experimental values. The systematic error in the experiment is, as discussed in Sec. IV B, estimated to be $<20\%$. The uncertainties in the calculated rate coefficients due to systematic errors are of the same order. Thus the observed difference can be attributed to the total systematic errors.

Field ionization limits the number of Rydberg states, which might survive the motional electric field in the dipole magnet and be detected, to a maximum n. From Eq. (7) n_{max} is estimated to be 16 in this experiment. However, recombined ions with $n > n_{max}$ can contribute to the DR spectrum if they decay radiatively to states with $n \leqslant n_{max}$ before the dipole magnet. How much the states with $n > n_{max}$ contribute will thus depend on the flight time of the ions from the interaction region to the dipole magnet. The distance between the center of the interaction region and the dipole magnet is about 1.6 m, and the ion velocity in the experiments was 3.9×10^7 m/s, which gives an average flight time of about 40 ns.

A ''delayed cutoff'' model accounting for the radiative decay of the Rydberg states was used in the AS calculations. The model was described in Ref. [7]. The calculations in Fig. 2 are made with flight times of 10, 20, 30, 40, and 50 ns. For the Rydberg resonances with $n > n_{max}$ a fairly good agreement between the experiment and the calculation using the estimated flight time of 40 ns is found. The delayed cutoff model thus seems to work quite well in this case.

For the studied system, the DR resonances closest to threshold, at low relative energies, are due to $2p5l$ states. Those resonances appear in a spectrum between 0.18 and 1.5 eV. All the three data sets measured cover this energy region, and they yield rate coefficient spectra which are in excellent agreement with each other. Figures 3, 4, and 5 show the experimental spectrum derived from one of the narrow data sets. The experimental spectrum is compared to the results from calculations using the four different models described in Sec. V. In Fig. 3 a comparison is made with the results from the two different calculations using the AUTOSTRUCTURE method, in Fig. 4 we show the results from the *R*-matrix method; and in Fig. 5 the results from the complex-rotation method.

The AUTOSTRUCTURE calculation performed within the *LS*-coupling scheme yields a result which is in rather poor agreement with experiment (see the upper part of Fig. 3). In *LS* coupling, transitions to the $2p5p\ ^{1,3}P$, $2p5d\ ^{1,3}D$, $2p5f\ ^{1,3}F$, and $2p5g\ ^{1,3}G$ doubly excited states are forbidden, since these states cannot be reached from the initial state conserving both parity and the orbital angular momentum L. However, the *LS*-forbidden transitions can give a significant contribution, which for example was shown in a previous measurement on C^{3+} [4] where, in fact, they gave rise to the strongest DR resonances. For N^{4+} it turns out that roughly one third of the DR strength for the $2p5l$ resonances is due to *LS*-forbidden transitions. Therefore, it is not that surprising that the *LS*-coupling method fails to reproduce the experimental spectrum.

The results from AS calculation using the Breit-Pauli approximation (see the lower part of Fig. 3) and *R*-matrix methods (Fig. 4) agree considerably better with experiment. These models seem to give a total strength which agrees with experiment. However, as is also the case for the *LS*-coupling results, the resonance positions do not match with the experimental ones. The difference in peak positions is in most cases well outside the experimental uncertainties and indicate that some correlation contributions are still missing. Furthermore, although the rate coefficients are in fairly good agreement overall, some of the peaks are underestimated and others appear to be overestimated in Figs. 3 and 4 (upper). Apart from the energy shift, the *R*-matrix results in Fig. 4 (lower) only differ noticeably from experiment for the peak centered at 1.2 eV, which is sensitive to resonance positions (i.e. mixing).

The results obtained with many-body perturbation theory combined with complex rotation, on the other hand, are in almost perfect agreement with experiment. The theoretical rate coefficients are slightly higher than the experimental ones, but the difference is well within the experimental uncertainties.

It should be noted that the natural widths have not been taken into account in the AS spectra shown in Fig. 3. The widths of the peaks in those theoretical spectra are only due to the instrumental resolution. A few of the lines, which are substantially broadened by their natural widths, therefore appear much sharper than in the experimental spectrum. Note also that, for the *R*-matrix method, contributions from both DR and RR are implicitly included in the method. For the other methods, an RR contribution has been added to the calculated DR spectra. The RR contribution was calculated as outlined in Sec. II, with $n_{max} = 16$.

The high accuracy of the many-body perturbation theory calculation is confirmed by the good agreement for the $2s\text{-}2p_{1/2}$ and $2s\text{-}2p_{3/2}$ splittings in N^{4+}, with the experimental values to within approximately 6×10^{-5}. The calculated splittings are 9.9766 and 10.0088 eV, and the experimental splittings are 9.97617 and 10.00824 eV. Note that the inclusion of radiative effects [35–37] is important to obtain such an agreement, since their contribution is one order of magnitude larger than the present difference between theory and experiment. The results of the complex-rotation calculation for the, in total, 50 $2p5l$ doubly excited states in N^{3+} are summarized in Table II. The states are denoted by their dominant configuration and an *LS* term. From optical data in the literature [21,38] it is possible to derive the resonance positions for 16 of these states. According to Ref. [38], the errors in the optical values should be less than 2 meV. We estimate that the errors in the resonance positions from the complex-rotation calculation are less than 2 meV as well. The differences between the calculated and optical values are less than the combined maximum error of 4 meV for all but one of the 16 resonances. For the $2p5s\ ^1P$ state the optical value is 0.4564 eV, whereas the calculated value is 0.3496

eV. The calculation shows that this state has a large natural width of 142 meV. The state, thus, gives rise to a very broad resonance in the recombination spectrum, which, because of its large width, is observed as a weak feature in our experimental spectrum. The position and width of this feature support the calculated results for the $2p5s\,^1P$ state. We conclude that the optical value for this state is wrong.

Furthermore, the J quantum number of the optically observed $2p5f\,^3P$ state at 1.2155 eV is not specified in the literature. From our calculated results we find that the state must have $J=2$, since only the $J=2$ state is close enough in energy, at 1.2139 eV, to fit the optical value.

In addition to the resonance positions, Table II also includes the natural widths, autoionization rates, radiative rates, and DR strengths for the 50 $2p5l$ states. It is interesting to note that, for states with different J's belonging to the same triplet term, the autoionization rates (and consequently also the widths) vary substantially if the transitions from $2p5l$ to the $1s^22s$ continuum are LS forbidden, whereas the rates are almost identical if the transitions are allowed. This reflects the fact that the autoionization rates for the ''forbidden states'' depend critically on the amount of mixing with ''allowed states'' with the same total angular momentum J.

VII. SUMMARY

We have measured the electron–ion recombination spectrum of N^{4+} with high resolution. The measured spectra have been compared to theoretical results obtained from four different methods. The complex-rotation method yields results which are in excellent agreement with the measured spectrum. Resonance positions, natural widths, autoionization rates, radiative rates, and DR strengths calculated with this method are presented for all the 50 $2p5l$ doubly excited states in N^{3+}. The resonance positions are also compared to those optical values which are available. The calculated positions are found to agree very well with these optical values, except for the $2p5p\,^1P$ state for which the literature value is concluded to be wrong.

We believe that the resonance positions from the complex-rotation calculation, in fact, are as good as the optical values in the literature. A conclusion supported by the excellent agreement with the resonance positions in our experimental DR spectrum. Our results thus provide energy levels for all 50 $2p5l$ levels in N^{3+} at the same accuracy as the currently available 16 levels.

ACKNOWLEDGMENTS

The authors would like to thank the staff at the Manne Siegbahn laboratory for their assistance in this experiment. This work was supported by the Swedish Natural Science Research Council (NFR) and the Knut and Alice Wallenberg foundation.

[1] J.B.A. Mitchell, C.T. Ng, J.L. Forand, D.P. Levac, R.E. Mitchell, A. Sen, D.B. Miko, and J.Wm. McGowan, Phys. Rev. Lett. **50**, 335 (1983).

[2] D.S. Belić, G.H. Dunn, T.J. Morgan, D.W. Mueller, and C. Timmer, Phys. Rev. Lett. **50**, 339 (1983).

[3] P.F. Dittner, S. Datz, P.D. Miller, C.D. Moak, P.H. Stelson, C. Bottcher, W.B. Dress, G.D. Alton, N. Nešković, and C.M. Fou, Phys. Rev. Lett. **51**, 31 (1983).

[4] S. Mannervik, D. DeWitt, L. Engström, J. Lidberg, E. Lindroth, R. Schuch, and W. Zong, Phys. Rev. Lett. **81**, 313 (1998).

[5] E. Lindroth *et al.* (unpublished).

[6] G. Gwinner, A. Hoffknecht, T. Bartsch, M. Beutelspacher, N. Eklöw, P. Glans, M. Grieser, S. Krohn, E. Lindroth, A. Müller, A.A. Saghiri, S. Schippers, U. Schramm, D. Schwalm, M. Tokman, G. Wissler, and A. Wolf, Phys. Rev. Lett. **84**, 4822 (2000).

[7] W. Zong, R. Schuch, H. Gao, D.R. DeWitt, and N.R. Badnell, J. Phys. B **31**, 3729 (1998).

[8] T. Bartsch, A. Müller, W. Spies, J. Linkemann, H. Danared, D.R. DeWitt, H. Gao, W. Zong, R. Schuch, A. Wolf, G.H. Dunn, M.S. Pindzola, and D.C. Griffin, Phys. Rev. Lett. **79**, 2233 (1997).

[9] T. Bartsch, S. Schippers, A. Müller, C. Brandau, G. Gwinner, A.A. Saghiri, M. Beutelspacher, M. Grieser, D. Schwalm, A. Wolf, H. Danared, and G.H. Dunn, Phys. Rev. Lett. **82**, 3779 (1999).

[10] W. Zong, R. Schuch, E. Lindroth, H. Gao, D.R. DeWitt, S. Asp, and H. Danared, Phys. Rev. A **56**, 386 (1997).

[11] T. Bartsch, S. Schippers, M. Beutelspacher, S. Böhm, M. Grieser, G. Gwinner, A.A. Saghiri, G. Saathoff, R. Schuch, D. Schwalm, A. Wolf, and A. Müller, J. Phys. B **33**, L453 (2000).

[12] S. Schippers, T. Bartsch, C. Brandau, A. Müller, G. Gwinner, G. Wissler, M. Beutelspacher, M. Grieser, A. Wolf, and R. A. Phaneuf (unpublished).

[13] G. Kilgus, D. Habs, D. Schwalm, A. Wolf, N.R. Badnell, and A. Müller, Phys. Rev. A **46**, 5730 (1992).

[14] C. Brandau, T. Bartsch, C. Böhme, F. Bosch, G. Dunn, B. Franzke, A. Hoffknecht, C. Knocke, H. Knopp, C. Kozhuharov, A. Krämer, P.H. Mokler, A. Müller, F. Nolden, S. Schippers, Z. Stachura, M. Steck, T. Stöhlker, T. Winkler, and A. Wolf, Phys. Scr. **T80B**, 318 (1999).

[15] P.F. Dittner, S. Datz, P.D. Miller, P.L. Pepmiller, and C.M. Fou, Phys. Rev. A **35**, 3668 (1987).

[16] L.H. Andersen, G-Y. Pan, H.T. Schmidt, M.S. Pindzola, and N.R. Badnell, Phys. Rev. A **45**, 6332 (1992).

[17] H. Poth, Phys. Rep. **196**, 135 (1990).

[18] H.A. Kramers, Philos. Mag. **46**, 836 (1923).

[19] F. Brouillard, in *Atomic and Molecular Processes in Controlled Thermonuclear Fusion*, edited by C. J. Joachain and D. E. Post (Plenum, New York, 1983).

[20] P. Glans, E. Lindroth, N. Eklöw, W. Zong, G. Gwinner, A.A. Saghiri, M. Pajek, H. Danared, and R. Schuch, Nucl. Instrum. Methods Phys. Res. B **154**, 97 (1999).

[21] NIST *Atomic Spectra Database*. (WWW published at http://physics.nist.gov/cgi-bin/AtData/main_asd.)
[22] N.R. Badnell, J. Phys. B **30**, 1 (1997).
[23] S. Salomonson and P. Öster, Phys. Rev. A **41**, 4670 (1990).
[24] E. Lindroth and J. Hvarfner, Phys. Rev. A **45**, 2771 (1991).
[25] P. G. Burke and K. A. Berrington *Atomic and Molecular Processes–an R-matrix Approach* (Institute of Physics Publishing, Bristol, 1993).
[26] M.S. Pindzola, N.R. Badnell, and D.C. Griffin, Phys. Rev. A **46**, 5725 (1992).
[27] E. Lindroth, Hyperfine Interact. **114**, 219 (1998).
[28] E. Lindroth, Phys. Rev. A **49**, 4473 (1994).
[29] D.R. DeWitt, E. Lindroth, R. Schuch, H. Gao, T. Quinteros, and W. Zong, J. Phys. B **28**, L147 (1995).
[30] For an account of the early contributions to the complex rotation method see the whole No. 4 issue of Int. J. Quantum Chem. **14** (1978).
[31] Y.K. Ho, Phys. Rev. A **23**, 2137 (1981).
[32] K.T. Chung and B.F. Davis, Phys. Rev. A **26**, 3278 (1982).
[33] I. Lindgren, J. Phys. B **7**, 2441 (1974).
[34] E. Lindroth and A.-M. Mårtensson-Pendrill, Phys. Rev. A **53**, 3151 (1996).
[35] W.R. Johnson and G. Soff, At. Data Nucl. Data Tables **33**, 405 (1985).
[36] D.K. McKenzie and G.W.F. Drake, Phys. Rev. A **44**, R6973 (1991).
[37] S.A. Blundell, Phys. Rev. A **46**, 3762 (1992).
[38] D.J. Michels, S.G. Tilford, and J.W. Quinn, J. Opt. Soc. Am. **61**, 625 (1971).